Supporting Information (SI)

Understanding the origin of high thermoelectric figure of merit of Zintl-phase KCaBi

Sampad Mandal, Atish Ghosh, and Pranab Sarkar*

Department of Chemistry, Visva-Bharati, Santiniketan, 731235, India

E-mail: pranab.sarkar@visva-bharati.ac.in

S1. Different Charge carrier scattering mechanisms:

The electronic transport properties were calculated by considering the electron-acoustic phonon (acoustic deformation potential), ionized impurity, and electron-optical phonon scattering mechanisms. Under this theoretical approach, the characteristic scattering rate of the charge carriers can be obtained by Matthiessen's rule : $\frac{1}{\tau}=\frac{1}{\tau_{ADP}}+\frac{1}{\tau_{IMP}}+\frac{1}{\tau_{POP}}$, where τ_{ADP}, τ_{IMP} and τ_{POP} are the relaxation time from acoustic deformation potential (ADP), ionized impurity (IMP), and polar-optical phonon scattering, respectively. The mode-dependent scattering rates are calculated using the *momentum relaxation time approximation* (MRTA) (for elastic processes like ADP and IMP scattering) and *self-energy relaxation time approximation* (SERTA) (for inelastic processes like POP scattering) to the Boltzmann transport equation (BTE) within the Born approximation.

For elastic scattering, the expression of relaxation time ($\tilde{\boldsymbol{\tau}}_{i\mathbf{k}}$) for state $|i\mathbf{k}\rangle$ under the MRT approximation can be written as

$$\tilde{\boldsymbol{\tau}}_{i\mathbf{k}}^{-1} = \int_{-\infty}^{+\infty} \sum_{j} \frac{d^3q}{\Omega_{BZ}} \Big[1 - \frac{\mathbf{v}_{i\mathbf{k}}\mathbf{v}_{j\mathbf{k}+\mathbf{q}}}{|\mathbf{v}_{i\mathbf{k}}|^2}\Big] \tilde{\boldsymbol{\tau}}_{i\mathbf{k}\to j\mathbf{k}+\mathbf{q}}^{-1} \tag{1}$$

where Ω_{BZ} is the volume of the first Brillouin zone, $\mathbf{v}_{i\mathbf{k}}$ and $\mathbf{v}_{j\mathbf{k}+\mathbf{q}}$ are group velocity of the charge carrier in the initial state $|i\mathbf{k}\rangle$ and final state $|j\mathbf{k}+\mathbf{q}\rangle$, respectively. $\tilde{\boldsymbol{\tau}}_{i\mathbf{k}\to j\mathbf{k}+\mathbf{q}}^{-1}$ is the partial decay rate for the elastic scattering from initial electronic state $|i\mathbf{k}\rangle$ to final electronic state $|j\mathbf{k}+\mathbf{q}\rangle$.

For inelastic scattering, the expression of relaxation time ($\boldsymbol{\tau}_{i\mathbf{k}}$) for state $|i\mathbf{k}\rangle$ under the SERT approximation can be written as

$$\boldsymbol{\tau}_{i\mathbf{k}}^{-1} = \int_{-\infty}^{+\infty} \sum_{j} \frac{d^3q}{\Omega_{BZ}} \boldsymbol{\tau}_{i\mathbf{k}\to j\mathbf{k}+\mathbf{q}}^{-1} \tag{2}$$

where Ω_{BZ} is the volume of the first Brillouin zone, $\boldsymbol{\tau}_{i\mathbf{k}\to j\mathbf{k}+\mathbf{q}}^{-1}$ is the partial decay rate for the inelastic scattering from the initial electronic state $|i\mathbf{k}\rangle$ to the final electronic state $|j\mathbf{k}+\mathbf{q}\rangle$.

S2. Phonon scattering mechanism and corresponding phase space

The lattice thermal conductivities were calculated considering the three-phonon scattering process, which obeys the energy and momentum conservation laws and can be defined as

$$\begin{aligned} \hbar\omega_{s''q''} &= \hbar\omega_{sq} \pm \hbar\omega_{s'q'} \\ \hbar q'' &= (\hbar q \pm \hbar q') \pm \hbar G \end{aligned} \tag{3}$$

where q'', q', and q are the wave vectors of the three phonons involved in the three-phonon scattering process and s'', s', and s are the modes of the corresponding three phonons. G is the reciprocal lattice vector, which is zero for normal processes (N-process) and non-

zero for Umklapp-processes (U-process). "+"and "-"correspond to the phonon absorption and emission processes, respectively. The total phase space available for the three-phonon scattering process can be defined as the sum of frequency-weighted sums over all possible modes N following the Bose-Einstein distribution function f

$$P_3 = P_3^+ + P_3^- \tag{4}$$

where

$$P_3^{\pm} = \frac{1}{2N} \sum_{s's''} \left\{ \begin{matrix} 2(f_{s'} - f_{s''}) \\ f_{s'} + f_{s''} + 1 \end{matrix} \right\} \frac{\delta(\omega_{sq} \pm \omega_{s'q'} - \omega_{s''q''})}{\omega_{sq}\omega_{s'q'}\omega_{s''q''}} \tag{5}$$

S3. Shifting of Fermi level at different charge carrier concentrations

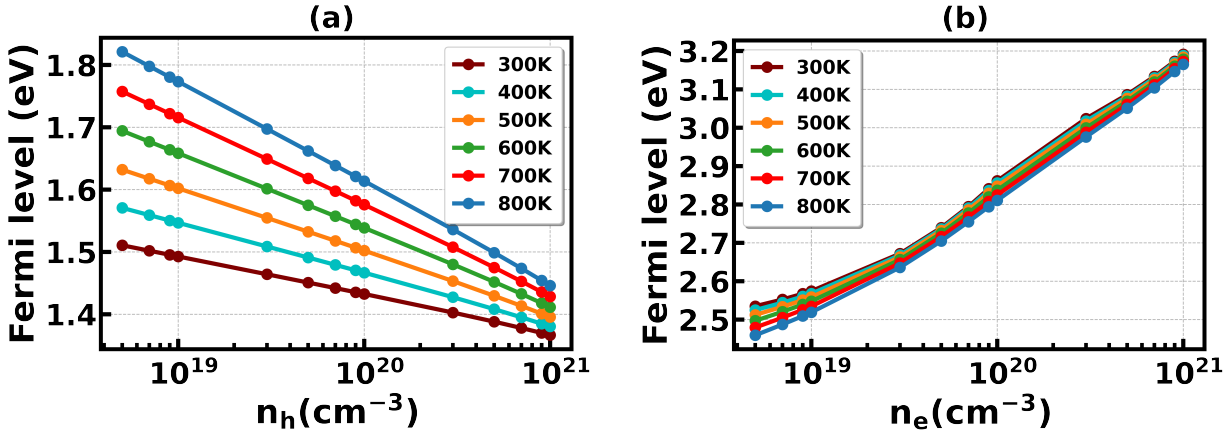

Figure S1: Shifting of Fermi level at different charge carrier concentrations for (a) p-type and (b) n-type KCaBi

S4. Convergence of lattice thermal conductivity at 300 K with respect to q-point grid

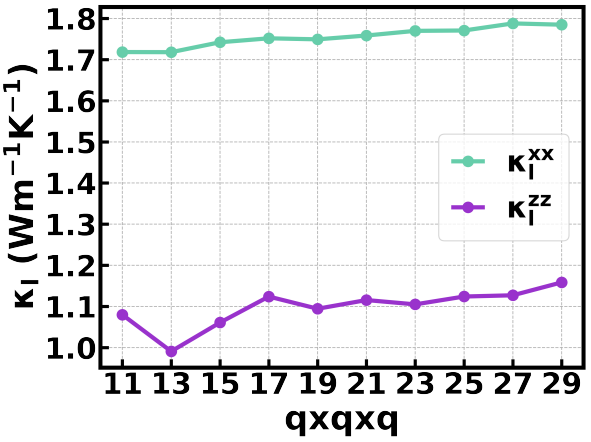

Figure S2: Convergence of lattice thermal conductivity at 300 K with respect to q-point grid

S5. AIMD at 800 K

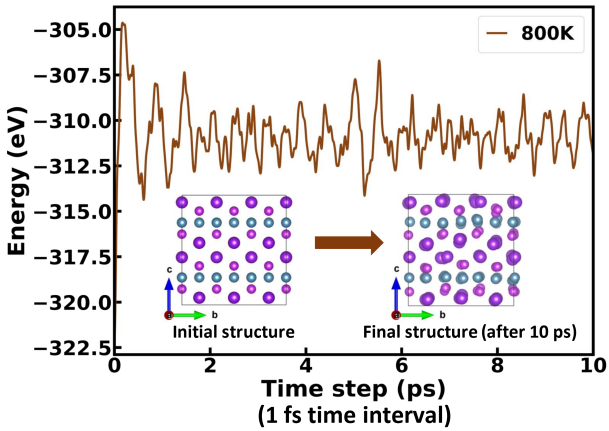

Figure S3: Plot of $2 \times 2 \times 2$ KCaBi supercell energy at different time step up to 20 ps for ab initio molecular dynamics simulation at 800 K

S6. Electron and hole effective masses along different K-path with respect to static mass of electron (m_e)

Table S1: Electron effective masses (m_e^*/m_e) along different K-path

Charge carrier	CBM-A	CBM-R	CBM-M	CBM-Y	CBM-Z
Electron effective mass (m_e^*/m_e)	0.140	0.146	0.132	0.132	0.199

Table S2: Hole effective masses (m_h^*/m_e) along different K-path

Charge carrier	VBM-A	VBM-R	VBM-M	VBM-Y	VBM-Z	VBM-Γ
Hole effective mass (m_h^*/m_e)	0.526	0.515	0.628	0.872	10.081	2.595

S7. Three-phonon phase space at 800 K

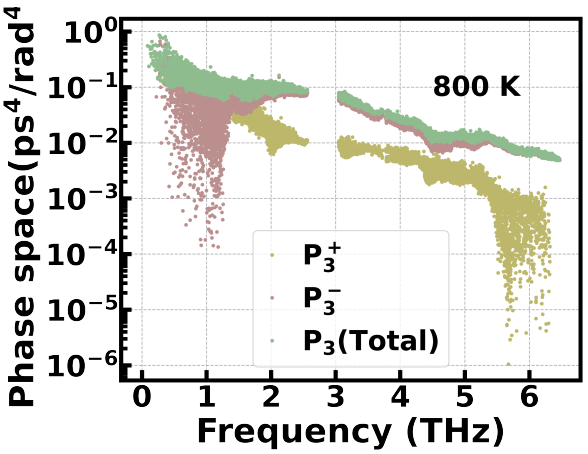

Figure S4: Three-phonon phase space at 800 K

S8. Phonon scattering rate at 800 K

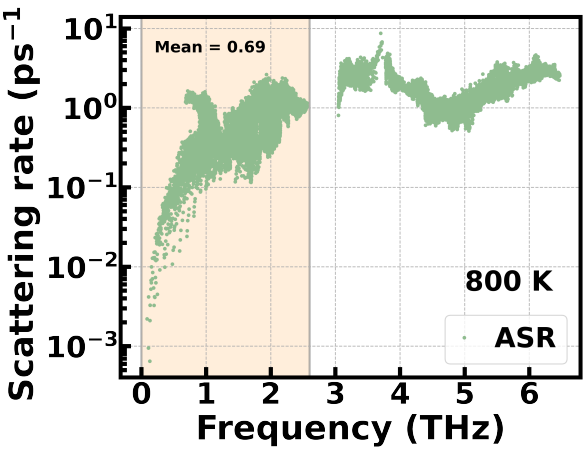

Figure S5: Phonon scattering rate for three-phonon scattering process at 800 K

S9. Charge carrier scattering rate for p-type KCaBi

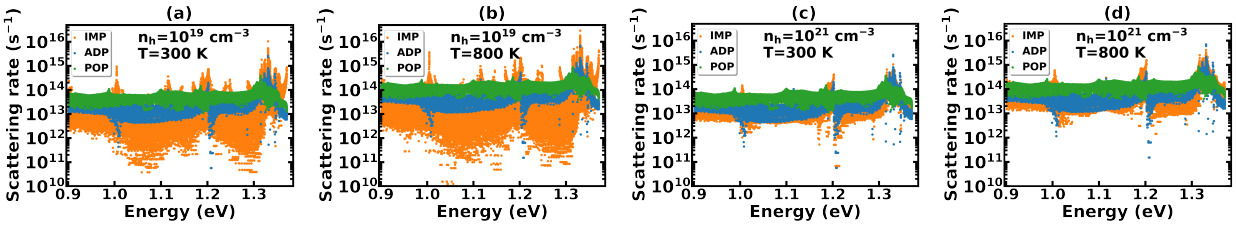

Figure S6: Hole scattering rates for hole concentration 10^{19} cm^{-3} at temperature (a) 300 K, (b) 800 K; and for 10^{21} cm^{-3} at temperature (c) 300 K, (d) 800 K, respectively, for p-type KCaBi.

S10. Charge carrier scattering rate for n-type KCaBi

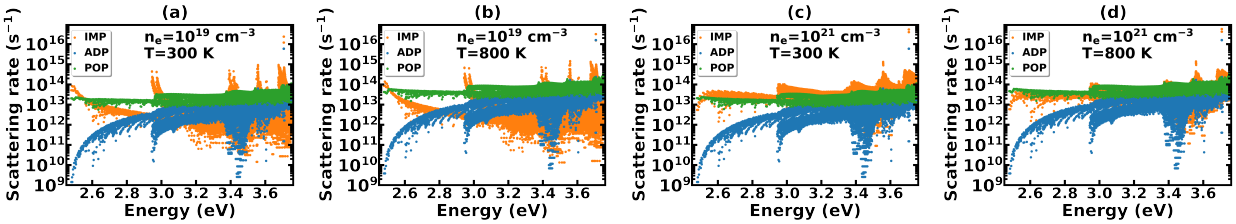

Figure S7: Electron scattering rates for electron concentration 10^{19} cm^{-3} at temperature (a) 300 K, (b) 800 K; and for 10^{21} cm^{-3} at temperature (c) 300 K, (d) 800 K, respectively, for n-type KCaBi.